Thermophysical properties and phase diagrams in the system MgO-SiO$_2$-FeO at upper mantle and transition zone conditions derived from a Multiple-Einstein method

M.H.G Jacobs[*1], Rainer Schmid-Fetzer[1], Arie P. van den Berg[2,3]

[1] Institute of Metallurgy, Clausthal University of Technology, Robert Koch Str. 42, 38678 Clausthal-Zellerfeld Germany

[2] Department of Earth Sciences, Utrecht University, Princetonlaan 8a, 3584 CB Utrecht, The Netherlands

[3] Faculty of Science, Vrije Universiteit Amsterdam, The Netherlands

* Corresponding author
Phone: +49-5323-722131
Fax: +49-5323-723120
Email: Michael.Jacobs@TU-Clausthal.de

Appendix A

Magnetic contributions to entropy and heat capacity
Developing the heat capacity expressed by eqn. (4) and (5) in McLaurin series results in:

$$C_V^\lambda (\tau \leq 1) = 2a_1 n_a R \sum_{j=0}^{\infty} \frac{\tau^{(2j+1)m}}{2j+1} \ln(1+\beta) \tag{14}$$

$$C_V^\lambda (\tau > 1) = 2a_2 n_a R \sum_{j=0}^{\infty} \frac{\tau^{-(2j+1)n}}{2j+1} \ln(1+\beta) \tag{15}$$

The coefficients a_1 and a_2 are found by making use of (1) that the magnetic entropy converges to $n_a R \ln(1+\beta)$ at infinite temperature and (2) by defining p as the fraction of the total energy above the critical temperature to transform the substance from one magnetic state to the other. That results in:

$$p = \frac{\int_{1}^{\infty} C_V^\lambda \, d\tau}{\int_{0}^{\infty} C_V^\lambda \, d\tau} \tag{16}$$

$$a_1 = m \left[1 - \cfrac{m}{\cfrac{s_2}{s_1}\left(1 - \cfrac{1}{p}\right)n + m} \right] \cfrac{1}{2 \displaystyle\sum_{j=0}^{\infty} \cfrac{1}{(2j+1)^2}} \tag{17}$$

$$a_2 = \left[\cfrac{m}{\cfrac{s_2}{s_1}\left(1 - \cfrac{1}{p}\right) + \cfrac{m}{n}} \right] \cfrac{1}{2 \displaystyle\sum_{j=0}^{\infty} \cfrac{1}{(2j+1)^2}} \tag{18}$$

In eqn. (17) and (18), s_1 and s_2 result from the integrations in (16) and are given:

$$s_1 = \sum_{j=0}^{\infty} \frac{1}{(2j+1)\left[(2j+1)m+1\right]} \tag{19}$$

$$s_2 = \sum_{j=0}^{\infty} \frac{1}{(2j+1)\left[-(2j+1)n+1\right]} \tag{20}$$

The entropy resulting from the integration of the heat capacity is:

$$S^\lambda (\tau \leq 1) = \frac{2a_1}{m} n_a R \sum_{j=0}^{\infty} \frac{\tau^{(2j+1)m}}{(2j+1)^2} \ln(1+\beta) \tag{21}$$

$$S^\lambda (\tau > 1) = n_a R \left(1 - \frac{2a_2}{n} \sum_{j=0}^{\infty} \frac{\tau^{-(2j+1)n}}{(2j+1)^2} \right) \ln(1+\beta) \tag{22}$$

In the Hillert-Jarl (1979) formalism, the magnetic contributions to thermodynamic properties are found by taking the first three terms in the series expansion. Their formalism is widely used in the Calphad community, such that entropy contribution of $-n_a R\ln(1+\beta)$ is negative at zero temperature and zero at infinite temperature. Because we prefer the third law to be valid, we have used the equations such that the entropy is zero at zero temperature and $+n_a R\ln(1+\beta)$ at infinite temperature commensurate with quantum mechanics.

The six 'd' electrons of Fe atoms in Fe_2SiO_4 and $FeSiO_3$ end members give rise to a net spin S=2 and it is expected that the magnetic moment equals 4. However, we noticed for fayalite ringwoodite and orthoferrosilite that the empirical formalism grossly overestimates the magnetic contribution to heat capacity when this value for the magnetic moment, β, is used, independent of the values that are used for p, m and n. Therefore we introduced a correction factor, m_f, in the magnetic Helmholtz energy contribution for these substances which is about 1/3 for fayalite and orthoferrosilite and 1/6 for ringwoodite and β is taken to be 4. Eqn. (6) becomes:

$$A^\lambda (T) = n_a \cdot g(\tau) \cdot m_f \cdot RT \ln(1+\beta) \tag{23}$$

Expressions for heat capacity and entropy are corrected, accordingly, with the same factor, m_f.

Coupling the Landau formalism to the Helmholtz free energy formalism
The Landau contribution to Gibbs free energy of α-quartz is given by eqn. (10) by adding the Landau contribution to the Gibbs free energy of β-quartz. The Landau contributions to other thermodynamic properties are given below.

Entropy

$$S^{Landau} = -\frac{1}{2} a_L Q^2 \tag{24}$$

Heat capacity

$$C_P^{Landau} = T \left(\frac{\partial S^{Landau}}{\partial T} \right)_P = \frac{a_L T}{4 T_c(P) Q^2} \tag{25}$$

Volume

$$V^{total} = V + V^{Landau} \tag{26}$$

$$V^{Landau} = -\frac{1}{2} a_L h Q^2 \left(1 - \frac{1}{3} Q^4 \right) \tag{27}$$

In eqn. (26), the volume V is calculated from the Helmholtz free energy expression, eqn. (1) as if no Landau contribution would be present.

Thermal expansivity
This property is derived from the expression of volume as:

$$\left(\frac{\partial V^{total}}{\partial T} \right)_P = \left(\frac{\partial V}{\partial T} \right)_P + \left(\frac{\partial V^{Landau}}{\partial T} \right)_P$$

$$\alpha^{total} = \frac{\alpha V + \alpha^{Landau} V^{Landau}}{V + V^{Landau}} \tag{28}$$

$$\alpha^{Landau} V^{Landau} = \frac{a_L h}{4 T_c(P)} (Q^{-2} - Q^2) \tag{29}$$

In eqn. (28), the volume V and thermal expansivity α are calculated from the Helmholtz free energy expression, eqn. (1) as if no Landau contribution would be present.

Bulk modulus
This property is derived from compressibility as:

$$\left(\frac{\partial V^{total}}{\partial P} \right)_T = \left(\frac{\partial V}{\partial P} \right)_T + \left(\frac{\partial V^{Landau}}{\partial P} \right)_T$$

$$K^{total} = \frac{V + V^{Landau}}{V/K + V^{Landau}/K^{Landau}} \tag{30}$$

$$V^{Landau}\Big/K^{Landau} = \frac{a_L\,Th^2}{4T_c^2(P)}(Q^{-2}-Q^2) \qquad (31)$$

Volume V and bulk modulus K are calculated from the Helmholtz free energy, eqn. (1), as if no Landau contribution would be present.

Entropy correction in the Landau formalism

Because the Landau contribution to the entropy of α-quartz is not zero at zero temperature, it violates the 3rd law of thermodynamics. To remedy this we added a value of $+0.5a_L$ to the entropy of both the low-temperature (α-quartz) and the high-temperature form (β-quartz). This has as effect that the transition entropy at the critical temperature remains zero, as is required in tricritical Landau theory. An additional effect is that the unstable disordered form (β-quartz) has a positive remnant entropy at zero temperature. The Gibbs energy of the low- and high-temperature form is consequently changed by $-0.5a_LT$. This treatment is not identical with implementing a Q^4 term in the Landau expression for the Gibbs energy, eqn. (12), by replacing this term by $-0.5a_L\{T_c(P)\text{-}T_c(P)Q^4\}$, by virtue of eqn. (13). The reason for that is that the order parameter, Q, has zero value for temperatures larger that the critical temperature. Therefore, construction of such a model would result in Gibbs energy values of $-0.5a_LT_c(P)$ instead of $-0.5a_LT$ above the critical temperature. The consequence is that the entropy at the critical temperature is $+0.5a_L$, whereas above the critical point it is zero, leading to a negative transition entropy when α-quartz transforms to β-quartz, which in turn is physically unrealistic. In this case it makes more sense to use the Landau expression for the Gibbs energy describing a first order transition in which the Q^4 term is present, such as we used in section 'Thermochemical data'. This, however, results in the same problem with the entropy, for which the treatment above can be applied.

The problem with entropy also occurs with the second order Landau expression for the Gibbs energy that we used in our previous description (Jacobs et al, 2017) for the phase boundary between SiO_2(Stishovite) and SiO_2(I, $CaCl_2$ structure). This boundary has a positive Clapeyron slope and both forms are stable at zero temperature. The situation differs from that described above in the sense that we did not apply an entropy correction. The reason for that is that the value of 0.013 J/K/mol for a_L is much smaller than the value 11.5 J/K/mol that we found for quartz. Neglecting the entropy correction results in a small negative entropy of SiO_2(I) of -0.0065 J/K/mol at zero Kelvin, which we found acceptable. Additionally, the small value for a_L has negligible effect on the phase boundary between SiO_2(I) and SiO_2(II, columbite), located parallel and at higher pressures relative to the Stishovite-SiO_2(I) boundary. This boundary was calculated by the intersection of the Gibbs energies of the two forms, and due to the small value of the entropy of SiO_2(I), a nearly horizontal departure of the boundary at zero temperature occurs, which is physically realistic.

Although the Landau formalism works well in the cases mentioned above, it might be anticipated that cases exist for which problems arise. These are most likely to occur for cases in which the two forms are both stable to very low temperatures combined with larger values for a_L, comparable with that of quartz.

Appendix B
Details of thermodynamic analyses of Fe_2SiO_4, $FeSiO_3$ polymorphs, coesite and quartz.

Polymorphs of Fe_2SiO_4 (fayalite, ringwoodite)
Fayalite is a crucial substance in the thermodynamic analysis of the system $FeO-SiO_2$ because its properties strongly constrain anharmonic and electronic effects of other substances, most directly those of ringwoodite and orthoferrosilite. For this substance the largest amount of datasets are available. A VDoS has been predicted by Yu et al. (2013) using ab initio. Although our method, using this VDoS, represents their predicted heat capacity well, experimental heat capacities are not represented to within reported uncertainty. Representing experimental low-temperature heat capacity data requires a shift in all frequencies in the VDoS of about -34 cm^{-1}, considerably larger than about 5 cm^{-1} that we needed for the magnesium end members including stishovite in our previous work of Jacobs et al (2017). The description for the crystal field electronic contribution has been kept the same as established by Aronson et al. (2007) and used by Jacobs and de Jong (2009). Figure 1 and Table 7 show that using the corrected VDoS, experimental low-temperature heat capacity and ambient entropy are represented to within experimental uncertainty. To represent thermal expansivity to within experimental uncertainty requires dispersion in Grüneisen parameters. It appears that dispersion in these parameters, partitioned in two frequency ranges, is sufficient to represent thermal expansivity data of Suzuki et al. (1981). Our values for Grüneisen parameters are based on those established by Jacobs et al. (2009), which in turn are based on IR spectroscopic data of Hofmeister (1987, 1989). Table 5 shows that, using data for heat capacity and thermal expansivity in the temperature range between 0 and 800 K, our analysis prefers the experimental adiabatic bulk modulus data of Isaak et al. (1993), measured between 300-500 K. These data are close to those of Sumino (1979), but deviate significantly from those of Graham et al. (1988). Jacobs and de Jong (2009) described fayalite with a vibrational model employing the quasi-harmonic approximation. Figure 2 shows that this model represents the data of Watanabe (1982), but it is insufficiently accurate to represent the drop calorimetric data of Orr (1953) and the more recent DSC and drop calorimetric data of Benisek et al. (2012). Benisek et al. (2012) measured larger heat capacity values than Watanabe (1982) in the range between 300 K and 800 K. We preferred their data, because in Jacobs et al. (2017) we found that Watanabe's (1982) measurements were also too small for wadsleyite and ringwoodite Mg_2SiO_4. From Figure 2 it is evident that finding a description consistent with the data of Benisek et al. (2012) requires an additional physical effect, for which we suggest intrinsic anharmonicity or an electronic contribution. A value of -2.93×10^{-5} K^{-1} for anharmonicity is required to describe the DSC data of Benisek et al (2012) in the range between 290 K and 800 K, a value about 2.5 times larger than for magnesium end members determined by Jacobs et al. (2017). In the alternative analysis, without including anharmonicity, a value of 2.418×10^{-3} $J/K^2/mol$ $FeSi_{0.5}O_2$ for the electronic coefficient, β_{el} in eqn. (3), must be used. In both cases, however, a significant deviation from the drop calorimetric data of Orr (1953) and Benisek et al (2012) above 800 K is still present. Benisek et al. (2012) discussed in their paper that data measured by Orr (1953) for forsterite and fayalite may be flawed by systematic errors in the temperature range between 500 K and 1400 K. Details concerning the causes for these systematic errors were not resolved in their paper. From our analyses it became clear that the data of Orr (1953) cannot be represented for temperatures between 300 K and 800 K, whereas the DSC data of Benisek et al. (2012) can be represented to within experimental uncertainty. To include the drop calorimetric heat content value $H_{1181}-H_{302}$ measured by Benisek et al. (2012) requires an additional modification in our model description, not possible to achieve by using anharmonicity or an electronic coefficient.

Nakamura and Schmalzried (1983) showed by thermo-gravimetric experiments that complicated point defects in fayalite occur above 1200 K. Instead of incorporating all different kind of point defects that they mention, which makes a calculation for the heat capacity quite tedious, we have opted for a more practical approach. We noticed that the remaining contribution to heat capacity above 800 K can be conveniently described by a mono-vacancy model suggested by Dorogokupets and Oganov (2007), and which they successfully employed to construct pressure scales of metallic elements, MgO and Ruby. The contribution to the Helmholtz energy due to these defects is written as:

$$A^{def}(T,V) = -\frac{3}{2} n_a RT \exp\left(s\eta^f - \frac{h\eta^g}{T} \right) \qquad (32)$$

In eqn. (32), h and s denote the enthalpy and entropy of the formation of a mono-vacancy, f and g are constants, n_a is the number of atoms in a molecular formula, and η denotes the compression V/V_0. Although this approach lacks some physical rigor, Figure 2 shows that it serves well to describe the heat capacity data of Orr (1953) above 1000 K. Moreover the calculated value 155.66 kJ/mol for the enthalpy difference H_{1181}-H_{302} represents the value 156.1±0.5 kJ/mol measured by Benisek et al. (2012) to within uncertainty.

The high-temperature heat capacity of fayalite has a large impact on the anharmonicity, or in our alternative description, on the electronic description of the iron end member of ringwoodite. Figure 3 shows that in the temperature range between 300 K and 800 K only heat capacity data measured by Watanabe (1982) are available to constrain anharmonicity or the electronic contribution. We anticipate that these data might be too low, just as we found for the wadsleyite and ringwoodite polymorphs of Mg_2SiO_4 and for fayalite. Therefore we used as constraint the Clapeyron slope of the phase boundary between fayalite and ringwoodite, depicted in Figure 2, and as we show below, we preferred that measured by Ono et al. (2013). Additionally, we established the description for heat capacity by using the VDoS predicted by Derzsi et al. (2011). They showed that their predicted isochoric heat capacity curve at 10 GPa represents the isobaric heat capacity curve established experimentally at 1 bar. Because heat capacity decreases with pressure, their predicted heat capacity curve at 1 bar is significantly larger than the experimental one. Applying this VDoS in our method, results in insignificantly different heat capacity as predicted by Derzsi et al. (2011). However, to represent low-temperature heat capacity data of Yong et al. (2007) requires a shift of the frequencies in the VDoS by about +14 cm^{-1}. In an aside analysis, we used the VDoS predicted by Yu et al. (2013), for which we found that a correction of about -35 cm^{-1} in the frequencies is required to represent heat capacity data, a value similar as we found for fayalite.

The behavior of heat capacity at temperatures below 50 K indicates that crystal field effects are present. Because no experimental data are available for electronic energy levels, required for the crystal field description, we optimized them using low temperature heat capacity data. The resulting parameters are given in Table 3. The first four energy levels effectively describe the heat capacity in the temperature range between 0 and 50 K. In that range the contribution due to lattice vibrations and the dilation term are negligible, and therefore these energy levels are robust. The e_g energy levels were arbitrarily set to 10^4 cm^{-1} and do not contribute significantly to thermodynamic properties. The intermediate energy levels at 1058 cm^{-1} were used to keep the anharmonicity parameter (or electronic coefficient in the alternative description) at about the same value as for fayalite. This value is not unambiguous because it is correlated with anharmonicity and the VDoS. This is seen, for example, when a simpler description is used in which the energy levels at 1058 cm^{-1} are omitted and all degeneracies are set equal to one. In that case the optimization leads to a value for anharmonicity of -

5.65×10^{-5} K^{-1}, a value considerably larger than the value of -2.93×10^{-5} K^{-1} for fayalite. Additionally the frequencies in the VDoS are displaced by about $+2$ cm^{-1} relative to the description employing the crystal field parameters in Table 3. However, this description may substitute that for the presently employed one without significant effect on the phase diagrams of Fe_2SiO_4 and $FeSiO_3$ and thermodynamic properties of ringwoodite.

In the present description for ringwoodite we employed Navrotsky's (1977,1994) model for taking cation disorder into account. This model is based on a cation exchange reaction in which Si^{4+} ions can move from tetrahedral sites to octahedral sites and Fe^{2+} ions from octahedral to tetrahedral sites. The model is characterized by one adjustable parameter, the interchange enthalpy. Based on structure refinements of Yagi et al. (1974), Navrotsky (1977) determined the value $+120.499$ kJ/mol for this property, which we kept fixed in our analysis. Just as our description for crystal field, cation disorder has the effect that anharmonicity has a similar value as that of fayalite. In an aside analysis, neglecting cation disorder, the analysis results in a value for anharmonicity of -3.5×10^{-5} K^{-1}. Also in this case the description may substitute the present description without affecting thermodynamic properties and phase diagrams.

We have directed our analyses to the phase boundary of Ono et al. (2013), depicted in Figure 2. The reason for that is that in this case enthalpy differences between ringwoodite and fayalite at 1 bar pressure represent the data in Table 6 to within experimental uncertainty. Figure 3 shows that, as a consequence, our calculated heat capacity systematically deviates from that measured by Watanabe (1982). Directing our optimization to phase boundaries determined by the other investigators given in Figure 2, results in even larger deviations from Watanabe's heat capacity. To constrain our analysis better requires new measurements of heat capacity above room temperature, determination of crystal field energies and Raman/IR spectroscopic measurements to establish values for intrinsic anharmonicity. Although it is possible to closely match the phase boundary of Ono et al. (2013), our analyses indicate that in that case the phase field coesite+ringwoodite in the phase diagram of $FeSiO_3$ extends far below 1473 K, which is not in accordance with findings of Akimoto (1970). This problem is detailed further in section 7 "phase diagrams".

The iron end member of wadsleyite is not stable and treated as a virtual end member. We employed the VDoS of Yu et al. (2013), and shifted its frequencies by -34 cm^{-1}, just as was necessary for fayalite and ringwoodite. We used thermal expansivity predicted by Yu et al. (2013) to determine Grüneisen and mode-q parameters. To establish values for the static volume, bulk modulus and its pressure derivative, we used experimental data of the wadsleyite solid solution phase. To avoid that this end member becomes stable at and below room temperature we employed the same expression for the crystal field contribution as for the ringwoodite form. To represent the phase diagram in Figure 1, we employed the regular solution model for olivine, wadsleyite and ringwoodite. It appeared to be sufficient to describe the excess Gibbs energies temperature independent. For olivine we adopted the excess enthalpy from Jacobs et al. (2009) and for ringwoodite we used the excess enthalpy determined experimentally by Akaogi et al. (1989). The excess enthalpy of wadsleyite and the reference energy of its iron end member were obtained by fitting the phase diagram data of Figure 1. Table 8 shows that excess Gibbs energy coefficients for the three solution phases are quite similar.

Polymorphs of FeSiO₃ (orthoferrosilite, low- and high-pressure clinoferrosilite)
For ortho-, HP- and LPclinoferrosilite no VDoS has been predicted by ab initio methods. Therefore we made use of the characteristic found by Yu et al. (2013) the VDoS of Fe_2SiO_4 end members resemble those of the Mg_2SiO_4 counter end members. Because iron atoms have

a larger mass than magnesium atoms, lattice vibrations in which iron atoms involved are located at lower frequencies than those involving magnesium atoms. Therefore we used the VDoS of the magnesium end members in our analyses, and displaced frequencies in it to lower values to represent the properties of the iron end members. To arrive at the simplest description we translated all frequencies in the VDoS of each end member. Although this operation also affects Si-O lattice vibrations located at high frequencies, we noticed that this does not significantly affects the representation of thermodynamic properties. Translations of typically -35 cm^{-1} were required for each of the three polymorphs.

Victor et al (2001) determined crystal field energies and degeneracies for two magnesium rich samples of orthopyroxene by combining results of their Mössbauer experiments and ligand field theory. For the iron end members of LP- and HPclinopyroxene, including that of orthopyroxene, these properties have not been measured. For orthoferrosilite we used their results for the $(Mg_{0.8}, Fe_{0.2})SiO_3$ sample. Although we expected that crystal field energies of orthoferrosilite are quite different, only small changes in the first four energy levels above the ground state of the M1 and M2 site were necessary to represent heat capacity measurements of Cemič and Dachs (2006), depicted in Figure 3. We treated the Grüneisen parameters of orthoferrosilite monodisperse, and determined them from the V-T measurements of Sueno et al. (1976), which are consistent with those of Yang and Ghose (1994) for orthopyroxene solid solutions, shown in Figure 4. Table 5 shows that static properties are determined accurately by bulk modulus measurements of Bass and Weidner (1984) and V-P measurements of Hugh-Jones (1997a).

Although model parameters for orthoferrosilite can be constrained reasonably well by experimental data, this is not the case for LP- and HPclinoferrosilite. Because no heat capacity measurements are available, we refrained from applying an arbitrary crystal field expression in the Helmholtz energy, although this contribution will certainly be present. For the two polymorphs, only single-crystal V-P measurements are available at room temperature, measured by Hugh-Jones et al. (1994). For LPclinoferrosilite V-T data were measured by Hugh-Jones (1997b). The only extra available data, constraining model parameters of the two polymorphs, are phase diagram data, shown in Figure 2. The large value for anharmonicity parameter (or electronic coefficient in the alternative description) of orthoferrosilite propagates into the parameters for LP- and HPclinoferrosilite, resulting in similar values as for orthoferrosilite. By using the phase boundary data between LPclino- and orthoferrosilite, our resulting 1 bar V-T behavior of LPclinoferrosilite necessarily deviates from that established experimentally by Hugh-Jones et al. (1997b), and it appears to be similar to that of orthoferrosilite. The reason for that is that we preferred the V-T data of orthoferrosilite measured by Sueno et al. (1976), which also deviate from those of Hugh-Jones (1997b), see Figure 4.

The Gibbs energies of $FeSiO_3$ end members are coupled to that of fayalite by magnesium-iron partitioning between olivine and orthopyroxene, shown in Figure 5. Using the thermophysical description for fayalite and orthoferrosilite, these data indicate that the excess Gibbs energy of orthopyroxene is almost zero at the conditions of the measurements of Seckendorff and O'Neill (1993), about 1273 K and 1.6 GPa. Although element partitioning over the M1 and M2 sites is present in orthopyroxene, we preferred a description based on a substitutional solution model rather than a sub lattice model. We constrained the value for excess entropy in Table 8 with data on excess enthalpy measured by Chatillon-Colinet et al. (1983).

Polymorphs of SiO₂ (quartz and coesite)

For quartz we used the VDoS predicted by Bosak et al. (2012). Representing low-temperature heat capacity of Westrum (1954), depicted in Figure 3 required a translation of the VDoS by

+15 cm^{-1}. We followed Holland and Powell (1998) to describe the ordering effect in α-quartz on thermodynamic properties by tricritical Landau theory. Optimizations using the quasi-harmonic approximation invariably led to a steep volume increase with temperature for β-quartz. To include the *V-T* behavior indicated by the data of Carpenter (1998), Bourova et al. (1998) and Ackerman et al. (1974), illustrated in Figure 4, required incorporation of volume dependent intrinsic anharmonicity in our model description. Representing all available data, results in a positive anharmonicity parameter that strongly depends on volume. That, in turn, results in negative Grüneisen parameters for temperatures above 1000 K where β-quartz is stable. Our results are in accordance with a conclusion of Welche et al. (1998), arrived at by a lattice dynamical method, that about one third of the vibrational modes in β-quartz have negative Grüneisen parameters, resulting in a decrease of volume when temperature increases. Although their work indicates dispersion in Grüneisen parameters, we kept our description monodisperse in Grüneisen and anharmonicity parameters, because dispersion in these parameters did not significantly affect the accuracy of representing thermodynamic properties. Static parameters were accurately constrained by ab initio calculations of the room-temperature isotherm by Kimizuka et al. (2007), which are in good agreement with the experimental data in Table 5 and Figure 4.

Wehringer et al. (2013) predicted a VDoS for coesite by combining results for diffuse and inelastic X-ray scattering experiments with ab initio lattice dynamics. Employing this VDoS results in heat capacities too low compared to experimental data. That also holds when the VDoS predicted by Keskar and Chelikowsky (1995) is employed. It appeared to be impossible to represent low-temperature heat capacity data of Atake et al (2000), Hemingway et al (1998) and Holm et al (1967) by shifting or stretching the VDoS, or by using dispersion in Grüneisen parameters. To represent the heat capacity data depicted in Figure 3 and the entropy at 298 K and 1 bar, we changed fractions in the VDoS. Model parameters were tightly constrained by *V-T* data at 1 bar and by *V-P* data at room temperature, given in Table 5 and shown in Figure 4. Because Skinner's (1962) ambient volume is 0.32% larger than that obtained by all other more recent measurements, we used their V/V_{297} data for constraining Grüneisen parameters. As shown in section 3 "thermochemical data" the phase boundary between quartz and coesite is extremely sensitive to the low-temperature heat capacity of coesite. Directing our description to the heat capacity data of Hemingway et al (1998) and Holm et al (1967) results in the phase boundary, labelled [H] in Figure 2, having a negative Clapeyron slope below 1000 K, incommensurate with all experimental datasets. In section "Thermochemical data" we detail that a positive Clapeyron slope of the phase boundary, commensurate with all datasets is obtained by directing our optimization towards the heat capacity of Atake et al (2000).

FeO

We treat the end member of ferropericlase as a stoichiometric compound FeO. Because our analysis is hampered by the fact that no direct data are available for it, we estimated most thermophysical properties from data of the solid solution phase (Mg,Fe)O. We estimated the VDoS for FeO by using an ab initio prediction of Wu et al. (2009) for (Mg$_{0.8125}$Fe$_{0.1875}$)O. Because adiabatic calorimetric heat capacity measurements of Stølen et al. (1996) for Fe$_{0.99}$O and heat capacity estimated by Grønvold et al. (1993) for FeO respectively are consistent with each other, we fine-tuned the VDoS to represent these data. Additionally we incorporated a crystal field contribution in our model description, which is based on energy levels measured by Schrettle et al (2012) obtained by FIR spectra, to arrive at the ambient entropy of 61±1 J/K/mol, commensurate with the calorimetric measurements. Ambient volume for FeO has been taken from Hentschel (1970) who claimed to have synthesized stoichiometric FeO.

Volumes of $(Mg_{1-x}Fe_x)O$ at 1 bar pressure show a linear behavior with composition between $x=0$ and about $x=0.5$, that extrapolates quite well to the ambient volume of Hentschel (1970) for FeO. Jacobsen et al. (2002) showed that volumes between $x=0.5$ and $x=1$ deviate from linear behavior, which is likely to be caused by a larger amount of Fe^{3+} in these mixtures, as shown in Table 1 of their work. Because we do not include Fe^{3+} in our model description, we assumed a linear behavior of volume in the entire composition range. Static properties were obtained from V-P-T and elasticity (K_s-P) measurements of $(Mg_{1-x}Fe_x)O$ mixtures, summarized in Table 5. Ferropericlase shows a spin transition between about 50 and 60 GPa, which we do not treat in the present work. Therefore we compare in Table 5 our results with experimental data for the high-spin configuration of ferropericlase for pressures up to 40 GPa. The representation of V-P data is generally comparable with the experimental uncertainty, which is typically between 0.2 and 0.5%. The exception is the representation of the data of Jacobsen et al. (2002), because their ambient volumes deviate slightly from the line connecting the volumes of the two end members. Their V/V_{300} data are, however, represented to within about 0.05%. Figure 5 shows that our description prefers adiabatic bulk modulus data of Jacobsen et al. (2002) for $(Mg_{1-x}Fe_x)O$ mixtures in which x varies between 0 and 0.8. It also illustrates that bulk modulus data of Jackson et al. (1978) show a marked increase with composition. However, in a later work, Jackson et al. (1990) showed that this trend may be an artefact of an improper procedure followed in the interpretation of their ultrasonic interferometric measurements. Our analysis of V-P-T data prefers the decreasing trend of bulk modulus with composition, in accordance with the majority of the investigations given in Figure 5. For that reason, our calculated V-P behavior of FeO at room temperature deviates from that obtained by databases of Fabrichnaya et al. (2004) and Stixrude et al. (2011), as shown in the inset of upper-right frame of Figure 5. However, Tables 1 and 2 include alternative analyses, in which the bulk modulus increases with composition, which is discussed in more detail in section 7 "phase diagrams". Following our previous work we have converted V-P-T measurements to a common pressure scale, that of Dorogokupets and Oganov (2007). This gives us the possibility to change our database in a transparent way when more accurate pressure scales become available. Our analysis reveals Grüneisen parameters for FeO that are insignificantly different from that of MgO, resulting in similar behavior of thermal expansivity of these two end members.

The determination of the phase boundary between the ringwoodite form of Fe_2SiO_4 and FeO + stishovite is not trivial procedure. In a first analysis we preferred the high-temperature heat capacity of Grønvold et al. (1993) depicted in Figure 5 to constrain the electronic coefficient of FeO. This choice produces in combination with our results for Fe_2SiO_4 ringwoodite the Clapeyron slope of the phase boundary determined by Matsuzaka et al (2000), depicted in Figure 2 for the phase diagrams of Fe_2SiO_4 and $FeSiO_3$. The Mg-Fe partitioning between the solid solution phases ringwoodite and ferropericlase, determined by Matsuzaka et al (2000) and Frost et al. (2001) in rhenium capsules, results in the reference energy of FeO, which completes the description of all model parameters for determining its Gibbs energy. By using the model parameters for stishovite determined by Jacobs et al (2017) and the ringwoodite form of Fe_2SiO_4, we arrived at the location of the phase boundary, representing the data of Matsuzaka to within 0.2 GPa between 1000 K and 1800 K. However, in section 7 "phase diagrams" we show in detail that consistency between heat capacity of FeO, Mg-Fe partitioning between the solid solutions ringwoodite and ferropericlase and phase diagram data depend on crucible material that has been used in the experiments.

Shear modulus

As shown by Jacobs et al (2017), for substances in the system MgO-SiO$_2$, our formalism does not allow putting tighter constraints to thermodynamic properties and phase diagrams by incorporating shear modulus data into the analyses. Therefore, these data were treated independently from the thermodynamic analyses. For all iron end members except for fayalite, insufficient data for shear modulus are available to achieve an unambiguous description for it. Therefore use has been made of shear modulus measurements of the solid solutions, such as for wadsleyite, ringwoodite and ferropericlase, described in section "constraints by solid solutions". For the iron end members of the solid solutions orthopyroxene, and LP- and HPclinopyroxene this was not possible. Therefore we were not able to achieve robust shear modulus descriptions for the iron end members of these phases. We consider them as estimates. We estimated shear modulus as follows. As shown in Table 5, shear modulus data for orthoferrosilite are only available at room temperature between 1 bar and 7 GPa to constrain its pressure derivatives. Because of the lack of data above room temperature we assumed the same temperature behavior at 1 bar pressure as orthoenstatite. For LP- and HPclinoferrosilite no data for shear modulus are available and therefore our description is based on properties of the magnesium counter end members. We made use of the Poisson value, v, which is related to adiabatic bulk modulus K_S and shear modulus G_{sh} by:

$$v = \frac{3K_S - 2G_{sh}}{2(3K_S + G_{sh})} \tag{33}$$

For LPclinoferrosilite we followed the same method that Jacobs et al (2017) used for LP clinoenstatite. We assumed that its Poisson value at ambient conditions is equal to that of orthoferrosilite. Because adiabatic bulk modulus is robust for LPclinoferrosilite, a value for its shear modulus at ambient conditions is thus achieved. Additionally, the 1-bar temperature behavior and the pressure behavior at room temperature is taken to be identical to that of LP clinoenstatite to determine temperature and pressure derivatives of shear modulus. To estimate the shear modulus of HPclinoferrosilite at ambient conditions, we assumed that the ratio of Poisson values at ambient conditions, v(HPcfs)/v(Ofs) has the same value as that for the magnesium counter end members. To determine shear modulus in *P-T* space, we assumed that the 1-bar temperature behavior and the pressure behavior at room temperature is identical to that of HPclinoenstatite. Because the solid solution HPclinopyroxene forms a stable assemblage at upper mantle conditions it is highly desirable to measure elastic parameters for this phase in the future.

Table 5 shows that the shear modulus of coesite was recently established by Chen et al (2015) between 1 bar and 13 GPa at room temperature. Because data above room temperature are absent we arbitrarily assumed a temperature derivative of about -0.01 GPa/K at 1 bar pressure. Coesite does not form a stable assemblage for overall compositions close to a pyrolytic mantle composition in the system MgO-SiO$_2$-FeO. That also holds for quartz. Because we are presently mainly interested in stable phase assemblages occurring in the upper mantle and transition zone, we have kept the shear modulus description for quartz simple. A more elaborate and more complicated description for its elasticity based on Landau theory is given by Carpenter et al (1998).

Table 1. Fractions in the VDoS of each substance, multiplied by 100. A 30-Einstein model has been used for all substances.

Fe$_2$SiO$_4$ (Fayalite)

1	0.0061	6	6.7919	11	3.1756	16	2.8090	21	0.0013	26	2.4900
2	0.9830	7	6.0721	12	2.0006	17	3.5725	22	0.0013	27	1.7461
3	4.0399	8	6.7826	13	5.0290	18	0.3554	23	0.4724	28	1.8976
4	6.5415	9	6.2934	14	6.0403	19	0.0013	24	7.0246	29	2.2289
5	7.4154	10	7.8991	15	2.7541	20	0.0013	25	4.9882	30	0.5855

Fe$_2$SiO$_4$ (ringwoodite)

1	0.0059	6	7.8002	11	5.3356	16	3.0167	21	0.1440	26	0.0191
2	0.1029	7	8.0122	12	7.2679	17	5.4696	22	0.0000	27	0.0353
3	0.3381	8	5.0004	13	7.8480	18	5.8324	23	0.0000	28	0.4216
4	1.7118	9	1.0591	14	6.5662	19	3.7901	24	0.0000	29	8.5346
5	5.4787	10	0.7878	15	2.2540	20	5.2515	25	0.0045	30	7.9116

Fe$_2$SiO$_4$ (wadsleyite)

1	0.0821	6	6.6582	11	5.2157	16	4.1668	21	0.8588	26	4.3378
2	0.6839	7	6.5961	12	5.7786	17	2.8171	22	0.0576	27	4.0713
3	2.1168	8	5.4788	13	4.8649	18	2.4458	23	0.6836	28	1.5239
4	5.5446	9	7.8295	14	3.8357	19	0.1105	24	1.6154	29	0.9564
5	6.2341	10	6.6994	15	5.8848	20	0.7504	25	1.5239	30	0.5775

FeSiO$_3$ (orthoferrosilite)

1	0.2613	6	5.8445	11	5.6087	16	1.9726	21	2.0721	26	2.7910
2	1.7100	7	6.7885	12	4.5946	17	2.4843	22	1.5970	27	1.7286
3	3.7007	8	6.5678	13	4.1223	18	3.1452	23	1.9343	28	0.6199
4	4.9757	9	5.9668	14	4.1790	19	3.0322	24	2.9241	29	0.5428
5	5.6571	10	6.0922	15	3.2223	20	2.9238	25	2.6747	30	0.2660

FeSiO$_3$ (HPclinoferrosilite)

1	0.8369	6	6.5078	11	4.9202	16	1.9449	21	1.9044	26	2.7034
2	3.4492	7	6.5554	12	4.0577	17	2.8700	22	1.4265	27	1.5123
3	4.7659	8	5.8913	13	4.1240	18	2.9918	23	2.3146	28	0.5926
4	5.4887	9	5.9538	14	3.6974	19	3.0375	24	2.7501	29	0.5495
5	5.5551	10	5.6654	15	2.4297	20	2.5700	25	2.6705	30	0.2633

FeSiO$_3$ (LPclinoferrosilite)

1	0.3856	6	5.4432	11	7.4646	16	0.4269	21	0.0933	26	1.6969
2	1.6945	7	5.4311	12	3.8479	17	1.6373	22	0.9894	27	4.1593
3	3.1067	8	7.4607	13	3.1007	18	2.4370	23	1.1652	28	4.3923
4	4.6090	9	7.6079	14	7.2986	19	2.5999	24	3.1474	29	1.0619
5	5.2883	10	6.8353	15	3.1190	20	0.3393	25	2.7402	30	0.4206

FeO

1	0.0015	6	0.5611	11	3.9411	16	5.7401	21	3.7914	26	1.7969
2	0.0357	7	0.8444	12	7.1428	17	9.9775	22	1.8482	27	1.4377
3	0.0959	8	1.2187	13	7.5748	18	13.4622	23	3.9643	28	1.1139
4	0.1994	9	1.7557	14	4.5511	19	9.9606	24	3.7641	29	0.7838
5	0.3561	10	2.5579	15	3.5300	20	5.3283	25	2.4257	30	0.2391

SiO$_2$ (quartz)

1	0.0423	6	4.7697	11	7.3460	16	1.3207	21	1.3416	26	2.3558
2	3.4804	7	5.1557	12	3.0129	17	0.7623	22	0.0024	27	8.6960
3	5.3813	8	5.3161	13	2.5072	18	2.2858	23	0.0000	28	1.7651
4	5.1216	9	3.6865	14	1.5716	19	2.7201	24	0.0000	29	7.1812
5	4.5989	10	6.6878	15	2.2858	20	8.1246	25	0.0005	30	2.4802

Table 1. (continued)

SiO$_2$ (coesite)											
1	0.0285	6	6.2514	11	4.3271	16	2.0052	21	0.2150	26	2.8680
2	1.5343	7	6.6515	12	2.9371	17	2.1395	22	0.1697	27	3.2025
3	4.9443	8	6.6606	13	1.9713	18	5.8375	23	0.5468	28	2.4075
4	5.7610	9	6.8828	14	2.3211	19	5.6056	24	3.3269	29	1.5923
5	5.6867	10	5.7474	15	2.3378	20	1.0592	25	4.7708	30	0.2106
Mg$_2$SiO$_4$ (forsterite)											
1	0.0380	6	5.6176	11	7.1524	16	3.8450	21	0.0427	26	2.5749
2	0.2729	7	5.0497	12	5.2327	17	3.6288	22	0.0100	27	2.0372
3	0.7307	8	6.0690	13	5.5834	18	3.1842	23	0.2940	28	2.0727
4	1.7042	9	7.6719	14	5.9776	19	0.1425	24	4.6687	29	2.9655
5	4.3832	10	7.5445	15	6.2537	20	0.0249	25	4.5304	30	0.6970

Table 2. Representation of experimental thermodynamic properties for polymorphs in the system FeO-SiO$_2$ and for compositions of solid solution phases in MgO-SiO$_2$-FeO. 'DO' indicates data are based on the pressure scale of Dorogokupets & Oganov (2007). Italicized references are ab initio results.

Property	Max. relative deviation in %	Average relative deviation in %	T-range in K	P-range in GPa	Reference
Fe$_2$SiO$_4$ (Fayalite)					
Volume	1.40	0.46	298	0.0-31.3	Zhang et al (2016)
	0.06	0.03	298	0.0-9.7	Zhang et al. (1998)
	2.01	0.15	298	0.0-10.6	Andrault et al (1995)
	0.52	0.25	673	4.6-6.2	Plymate & Stout (1990)
	2.57	0.86	300	9.5-37.3	Williams et al (1990)
	0.15	0.11	1273	3.9-6.2	Yagi et al (1987)
	0.89	0.29	298	0.0-14.0	Kudoh & Takeda (1986)
	0.46	0.43	296	0.0-4.2	Hazen (1977)
	0.29	0.15	296±3	0.0-7.3	Yagi et al (1975)
	0.02	0.02	323-1123	0.0	Suzuki et al (1981)
	0.22	0.11	293-1173	0.0	Smyth et al (1975)
α	2.90	1.05	323-1123	0.0	Suzuki et al (1981)
K_S	0.31	0.22	298	0.0-10.0	Speziale et al. (2004)
	0.14	0.32	300-500	0.0	Isaak et al (1993)
	3.10	3.10	298	0.0	Wang et al. (1989)
	13.90	9.32	273-1000	0.0	Graham et al. (1988)
	1.23	1.03	298-673	0.0	Sumino (1979)
Vp	0.39	0.20	300-500	0.0	Isaak et al (1993)
	4.78	2.79	273-1000	0.0	Graham et al (1988)
	0.91	0.41	298-673	0.0	Sumino et al (1979)
Vs	0.32	0.19	300-500	0.0	Isaak et al (1993)
	2.97	1.09	273-1000	0.0	Graham et al (1988)
	1.50	0.62	298-673	0.0	Sumino et al (1977)
Fe$_2$SiO$_4$ (Ringwoodite)					
Volume	0.09	0.05	298	0.0-10.2	Nestola et al (2010)
	1.22	0.49	673	4.5-24.2	Plymate & Stout (1994)
	0.09	0.07	298	0.0-4.8	Hazen (1993)
	0.47	0.19	773-1473	4.3-6.3	Yagi et al (1987)
	0.08	0.05	298	0.0-4.0	Finger et al (1979)
	0.99	0.22	298	0.0-25.5	Mao et al (1969)
	0.25	0.10	294-670	0.0	Mao et al. (1969)
α	20.0	11.9	273-2273	0.0	Suzuki (1979)
K_S	1.44	1.44	298	0.0	Rigden et al (1991)
	5.70	5.70	298	0.0	Liebermann et al (1975)
	0.53	0.53	298	0.0	Akimoto (1972)
	3.82	3.82	298	0.0	Mizutani et al (1970)
G_{Shear}	21.2	21.2	298	0.0	Rigden et al (1991)
	27.7	27.7	298	0.0	Liebermann et al (1975)
	17.6	17.6	298	0.0	Akimoto (1972)
FeSiO$_3$ (Orthoferrosilite)					
Volume	0.64	0.20	293-901	0.0	Hugh-Jones (1997b)
	0.06	0.02	297-1253	0.0	Sueno et al (1976)
	0.08	0.05	298	0.0-5.4	Hugh-Jones et al (1997a)
K_S	0.03	0.03	298	0.0	Bass & Weidner (1984)
G_{shear}	1.63	0.56	298	0.0-7.1	Kung et al (2014)

Table 2. (continued)

Property	Max absolute deviation in %	Average absolute deviation in %	*T*-range in K	*P*-range in GPa	Reference
	0.00	0.00	298	0.0	Bass & Weidner (1984)
FeSiO₃ (HPclinoferrosilite)					
Volume	0.09	0.04	298	0.0-4.3	Hugh-Jones et al (1994)
FeSiO₃ (LPclinoferrosilite)					
Volume	0.05	0.02	298	0.0-1.4	Hugh-Jones et al (1994)
SiO₂ (quartz)					
Volume	0.09	0.05	298	0.0-20.0	*Kimizuka et al (2007)*
	1.10	0.43	298	10.7-19.8	Kingma (1994)
	0.79	0.46	298	0.0-6.1	Levien et al (1980)
	0.21	0.09	298	0.0-2.82	Jorgensen et al (1978)
	1.17	0.45	298	0.0-7.3	d'Amour et al (1979)
	1.04	0.61	298	0.0-15.3	Hazen et al (1989)
	1.35	0.78	298	0.0-12.07	Olinger et al (1976)
K_S	34.0	4.40	292-969	0.0	Ohno et al (2006)
	34.0	4.30	850-1070	0.0	Kammer et al (1948)
	9.70	6.82	298	0.0-10.2	Wang et al (2015)
G_{shear}	4.86	1.57	292-970	0.0	Ohno et al (2006)
	1.34	1.12	298	0.0-10.2	Wang et al (2015)
SiO₂ (coesite)					
Volume	0.14	0.05	298	0.0-8.7	Angel et al. (2003)
	0.11	0.05	299-1200	0.0	Bourova et al (2002)
	0.08	0.03	298	0.0-9.6	Angel et al (2001)
	0.79	0.75	298	14.0-24.3	Hemley et al. (1988)
	0.06	0.02	105-603	0.0	Galkin et al (1987)
	0.26	0.09	298	0.0-5.2	Levien et al (1981)
	0.16	0.09	297-1317	0.0	Skinner (1962)
K_S	3.00	3.00	298	0.0	Weidner & Carleton (1977)
G_{shear}	0.0	0.0	298	0.0	Weidner & Carleton (1977)
	0.67	0.29	300	0-12.6	Chen et al (2015)
Ferropericlase (Mg₁₋ₓ,Feₓ)O					
Volume					
x(Fe)=0.06	0.39	0.30	298	32.5-40	Crowhurst et al (2008) DO
	0.13	0.067	298	0.0-40.0	Jackson et al (2006), DO
*x(*Fe*)*=0.10	0.49	0.21	298	0.0-40.0	Marquardt et al (2009), DO
*x(*Fe*)*=0.17	0.60	0.30	298	0.0-40.0	Lin et al (2005), DO
	0.60	0.28	300-700	0.0-40.0	Ito et al (2010), DO
*x(*Fe*)*=0.17	0.35	0.15	300-1100	0.0-40.0	Matsui et al (2012), DO
*x(*Fe*)*=0.20	1.40	0.60	298	0.0-40.0	Fei et al (2007), DO
*x(*Fe*)*=0.25	0.27	0.15	300-1100	0.0-40.0	Matsui et al (2012), DO
*x(*Fe*)*=0.27	0.21	0.17	298	0.0-40.0	Jacobsen et al (2002), DO
*x(*Fe*)*=0.35	0.65	0.25	298	0.0-40.0	Chen et al (2012), DO
*x(*Fe*)*=0.39	0.30	0.19	298	0.0-40.0	Fei et al (2007), DO
*x(*Fe*)*=0.40	0.55	0.28	298	0.0-40.0	Lin et al (2005), DO
*x(*Fe*)*=0.402	0.42	0.14	298-1273	0.0-10.0	Zhang et al. (2002), DO
*x(*Fe*)*=0.402	0.28	0.08	298-700	8.0-30.0	Fei et al. (1992), DO
*x(*Fe*)*=0.56	1.07	0.60	298	0.0-40.0	Jacobsen et al (2002), DO
*x(*Fe*)*=0.58	0.94	0.75	298	0.0-40.0	Fei et al (2007), DO
K_S(*x*=0.06)	2.23	1.83	298	0.0-40.0	Crowhurst et al (2008) DO

Table 2. (continued)

Property	Max absolute deviation in %	Average absolute deviation in %	*T*-range in K	*P*-range in GPa	Reference
$K_S(x=0.06)$	4.22	2.31	298	0.0-40.0	Jackson et al (2006) DO
$K_S(x=0.10)$	3.68	2.79	298	0.0-40.0	Marquardt et al (2009) DO
$K_S(x=0.35)$	5.89	3.32	298	0.0-40.0	Chen et al (2012) DO
$G_S(x=0.06)$	4.59	3.36	298	0.0-40.0	Crowhurst et al (2008) DO
$G_S(x=0.06)$	2.09	0.83	298	0.0-40.0	Jackson et al (2006) DO
$G_S(x=0.10)$	5.42	2.10	298	0.0-40.0	Marquardt et al (2009) DO
$G_S(x=0.17)$	4.78	4.22	298	0.0-40.0	Kung et al (2002) DO
Olivine (Mg$_{1-x}$Fe$_x$)$_2$SiO$_4$					
Volume					
$0.08<x<0.38$	0.20	0.20	298	0.0-8.2	Nestola et al (2011)
If *V/V(P=0)*	0.09	0.03	298	0.0-8.2	
x(Fe)=0.10	0.52	0.17	298	0.0-32.4	Zha et al (1998)
x(Fe)=0.10	0.09	0.04	298	0.0-15.0	Abramson et al (1997)
$K_S(x=0.10)$	5.07	1.81	298-900	0.0-19.0	Mao et al (2015)
$K_S(x=0.125)$	1.15	0.48	298-1700	0.0-20.0	*Núñez et al (2012)*
$K_S(x=0.10)$	4.00	1.37	298	0.0-7.1	Darling et al (2004)
$K_S(x=0.10)$	5.63	2.65	298	0.0-32.4	Zha et al (1998)
$K_S(x=0.10)$	0.71	0.40	298	0.0-15.0	Abramson et al (1997)
$K_S(x=0.10)$	2.19	0.77	298	0.0-13.0	Zaug et al (1993)
$K_S(x=0.10)$	0.94	0.58	300-1500	0.0	Isaak et al (1992)
$G_S(x=0.10)$	3.22	1.71	298-900	0.0-19.0	Mao et al (2015)
$G_S(x=0.125)$	7.89	2.16	298-1700	0.0-20.0	*Núñez et al (2012)*
$G_S(x=0.10)$	2.34	1.39	298	0.0-7.1	Darling et al (2004)
$G_S(x=0.10)$	6.61	2.83	298	0.0-32.4	Zha et al (1998)
$G_S(x=0.10)$	2.67	2.14	298	0.0-15.0	Abramson et al (1997)
$G_S(x=0.10)$	5.44	1.90	298	0.0-13.0	Zaug et al (1993)
$G_S(x=0.10$	2.00	1.53	300-1500	0.0	Isaak et al (1992)
H^{excess}	136	40	975	0.0	Wood & Kleppa (1981)
	23	11	975	0.0	Kojitani et al (1994)
V^{excess}	217	47	293	0.0	Schwab & Küstner (1977)
	60	37	293	0.0	Fisher & Medaris (1969)
Wadsleyite (Mg$_{1-x}$Fe$_x$)$_2$SiO$_4$					
Volume					
x(Fe)=0.16	0.28	0.15	300-808	0.0-28.0	Fei et al (1992), DO
$K_S(x=0.12)$	0.41	0.29	300-1000	0.0-20.0	Sinogeikin et al (2003)
$K_S(x=0.125)$	0.55	0.27	300	0.0-30.0	*Núñez et al (2012)*
$K_S(x=0.075)$	2.26	1.42	300	0.0-17.7	Wang et al (2014)
$K_S(x=0.12)$	2.22	1.46	300	0.0-9.6	Li et al (2000)
$G_S(x=0.075)$	1.97	0.63	300	0.0-17.7	Wang et al (2014)
$G_S(x=0.075)$	0.56	0.20	300-1000	0.0-20.0	Sinogeikin et al (2003)
$G_S(x=0.125)$	9.02	6.90	300	0.0-20.0	*Núñez et al (2012)*
$G_S(x=0.12)$	0.27	0.19	300-1000	0.0-20.0	Sinogeikin et al (2003)
$G_S(x=0.12)$	0.77	0.43	300	0.0-9.6	Li et al (2000)
Ringwoodite (Mg$_{1-x}$Fe$_x$)$_2$SiO$_4$					
Volume					
$0\leq x\leq 1$	0.48	0.26	293	0.0-4.8	Hazen et al (1993)
$x=0.4, x=0.6$	0.21	0.09	294-1041	0.0	Ming et al (1992)
$K_S(x=0.09)$	2.23	0.71	295-923	0.0-15.8	Sinogeikin et al (2003)
$K_S(x=0.09)$	1.22	0.88	300-470	0.0	Mayama et al (2005)

Table 2. (continued)

Property	Max absolute deviation in %	Average absolute deviation in %	T-range in K	P-range in GPa	Reference
$K_S(x=0.125)$	2.05	0.80	300-2000	0.0-30.0	*Núñez et al (2012)*
$K_S(x=0.25)$	2.59	2.59	300	0.0	Sinogeikin et al (1997)
$G_S(x=0.09)$	1.66	1.02	295-923	0.0-15.8	Sinogeikin et al (2003)
$G_S(x=0.09)$	0.44	0.39	300-470	0.0	Mayama et al (2005)
$G_S(x=0.125)$	9.62	2.26	300-2000	0.0-30.0	*Núñez et al (2012)*
$G_S(x=0.25)$	0.03	0.03	300	0.0	Sinogeikin et al (1997)
H^{excess}	14.1	14.1	975	0.0	Akaogi et al (1989)
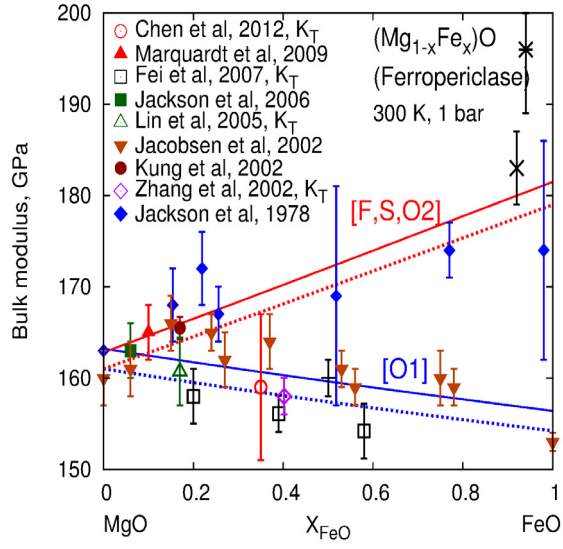
Fig 1. solid (dashed) curves represent adiabatic (isothermal) bulk modulus, and solid (open) symbols represent adiabatic (isothermal) bulk modulus. Labels [F,S] represent results obtained with databases of Fabrichnaya et al. (2004) and Stixrude & Lithgow-Bertelloni (2011). Labels [O1] and [O2] denote our own results. Additional data are from x: Dimshits et al (2018), +: Solmatov et al (2016), *: Wicks et al (2015)

References

Abramson EH, Brown JM, Slutsky LJ, Zaug J (1997) The elastic constants of San Carlos olivine to 17 GPa. J Geophys Res B 102:12253-12263

Akimoto S (1972) the system MgO-FeO-SiO_2 at high pressures and temperatures – phase equilibria and elastic properties. Tectonophysics 13:161-187

Andrault D, Bouhifd MA, Itié JP, Richet P (1995) Compression and amorphization of $(Mg,Fe)_2SiO_4$ olivines: An X-ray diffraction study up to 70 GPa. Phys Chem Minerals 22:99-107

Bass JD, Weidner DJ (1984) Elasticity of single crystal orthoferrosilite. J Geophys Res B 89:4359-4371

Bosak A, Krisch M, Chernishov D, Winkler B, Milman V, Refson K, Schulze-Brieze C (2012) New insights into the lattice dynamics of α-quartz. Z Kristallogr 227:84-91

Carpenter MA, Ekhard KH, Salje EKH, Graeme-Barber A, Wruck N, Dove MT, Knight KS (1998) Calibration of excess thermodynamic properties and elastic constant variations associated with the $\alpha \leftrightarrow \beta$ phase transition in quartz. Am Mineral 83:2-22

Chatillon-Colinet C, Newton RC, Perkins D III (1983) Thermochemistry of $(Fe^{2+},Mg)SiO_3$ orthopyroxene. Geochim Cosmochim Acta 47:1597-1603

Chen B, Jackson JM, Sturhahn W, Zhang D, Zhao J, Wicks JK, Murphy CA (2012) Spin crossover equation of state and sound velocities of $(Mg_{0.65}Fe_{0.35})$ ferropericlase to 140 GPa. J Geophy Res B 117:08208, 9pp

Chen T, Gwanmesia GD, Wang X, Zou Y, Liebermann RC, Michaut C, Li B (2015) Anomalous elastic properties of coesite at high pressure and implications for the upper mantle X-discontinuity. Earth Planet Sci Lett 412:42-51

Crowhurst JC, Brown JM, Goncharov AF, Jacobsen SD (2008) Elasticity of (Mg,Fe)O through the spin transition of iron in the lower mantle. Science 319:451-453

Darling KL, Gwanmesia GD, Kung J, Li B, Liebermann RC (2004) Ultrasonic measurements of the sound velocities in polycrystalline San Carlos olivine in multi-anvil, high-pressure apparatus. Phys Earth Planet Int 143-144: 19-31

Derzsi M, Piekarz P, Tokár K, Jochym PT, Łażewski J, Sternik M, Parlinski K (2011) Comparative ab initio study of lattice dynamics and thermodynamics of Fe_2SiO_4- and Mg_2SiO_4-spinels. J Phys Condens Mat 23:105401 (1-6)

Dorogokupets PI, Oganov AR (2007) Ruby, metals, and MgO as alternative pressure scales: a semiempirical description of shockwave, ultrasonic, x-ray, and thermochemical data at high temperatures and pressures. Phys Rev B 75:024115

Dymshits AM, Litasov KD, Shatskiy A, Chanyshev AD, Podborodnikov IV, Higo Y (2018) Phase boundary between cubi B1 and rhombohedral structures in (Mg,Fe)O magnesiowüstite determined by in situ X-ray diffraction measurements. Phys Chem Minerals 45:51-58

Fei Y, Mao H-k, Shu J, Hu J (1992) P-V-T equation of state of magnesiowüstite $(Mg_{0.6}Fe_{0.4})$O. Phys Chem Minerals 18:416-422

Fei Y, Zhang L, Corgne A, Watson H, Ricolleau A, Meng Y, Prakapenka V (2007) Spin transition and equations of state of (Mg,Fe)O solid solutions. Geophys Res Lett 34:L17307, 5pp

Finger L, Hazen RM, Yagi T (1979) Crystal structure and electron densities of nickel and iron silicate spinels at elevated temperature and pressure. Am Mineral 64:1002-1009

Fisher GW, Medaris LG (1969) Cell dimensions and x-ray determinative curve for synthetic Mg-Fe olivines. Am Mineral 54:741-753

Galkin VM, Doroshev AM, Babich Yu V (1987) Thermal expansion of coesite. GeoKhimiya 11:1645-1647

Graham E, Schwab JA, Sopkin SM, Takei H (1988) The pressure and temperature

dependence of the elastic properties of single-crystal fayalite Fe_2SiO_4. Phys Chem Minerals 16:186-198

Hazen RM (1977) Effects of temperature and pressure on the crystal structure of ferromagnesian olivine. Am Mineral 62:286-295

Hazen RM (1993) Comparative compressibilities of silicate spinels: anomalous behavior of $(Mg,Fe)_2SiO_4$. Science 259:206-209

Hentschel B (1970) Stoiciometric FeO as metastable intermediate of the decomposition of Wustite at 225 °C. Z Naturforsch A 25:1996-1997

Hofmeister AM (1987) Single-crystal absorption and reflection infrared spectroscopy of forsterite and fayalite. Phys Chem Minerals 14:499-513

Hofmeister AM, Xu J, Mao H-K, Bell PM, Hoering TC (1989) Thermodynamics of Fe-Mg olivines at mantle pressures: mid- and far-infrared spectroscopy at high pressure. Am Miner 74:281-306

Hugh-Jones DA, Chopelas A, Angel RJ (1997a) Tetrahedral compression in $(Mg,Fe)SiO_3$ orthopyroxenes. Phys Chem Minerals 24:301-310

Isaak DG (1992) High-temperature elasticity of iron-bearing olivines. J Geophys res B 97:1871-1885

Ito E, Yoshino T, Yamazaki D, Shatskiy AS, Shan S, Guo X, Katsura T, Higo Y, Funakoshi K (2010) High pressure generation and investigation of the spin transition of ferropericlase $(Mg_{0.83}Fe_{0.17})O$. J Phys Conf Ser 215:012099

Jackson I, Liebermann RC, Ringwood AE (1978) Elastic properties of $(Mg_xFe_{1-x})O$ solid solutions. Phys Chem Minerals 3:11-31

Jackson I, Khanna SK (1990) Elasticity, shear mode softening and high-pressure polymorphism of wüstite $(Fe_{1-x}O)$. J Geophys Res B 95:21671-21685

Jackson JM, Sinogeikin SV, Jacobsen SD, Reichmann HJ, Mackwell SJ, Bass JD (2006) Single-crystal elasticity and sound velocities of $(Mg_{0.94}Fe_{0.06})O$ ferropericlase to 20 GPa. J Geophy Res B 111:09203, 8pp

Keskar NR, Chelikowsky JR (1995) Calculated thermodynamic properties of silica polymorphs. Phys Chem Minerals 22:223-240

Kudoh Y, Takeda H (1986) Single-crystal X-ray diffraction study on the bond compressibility of fayalite, Fe_2SiO_4 and rutile, TiO_2 under high pressure, Physica 139&140B:333-336

Kung J, Li B, Weidner DJ, Zhang J, Liebermann RC (2002) Elasticity of $(Mg_{0.83}Fe_{0.17})O$ ferropericlase at high pressure: ultrasonic measurements in conjunction with X-radiation techniques. Earth Planet Sci Lett 203:557-566

Kung J, Li B (2014) Lattice dynamic behavior of orthoferrosilite $(FeSiO_3)$ toward phase transition under compression. J Phys Chem C 118:12410-12419

Li B, Liebermann RC (2000) Sound velocities of wadsleyite β-$(Mg_{0.88}Fe_{0.12})SiO_4$ to 10 GPa. Am Mineral 85:292-295

Liebermann RC (1975) Elasticity of olivine (α), beta (β), and spinel (γ) polymorphs of germanates and silicates. Geophys J Roy Astr Soc 42:899-929

Lin J-F, Struzhkin VV, Jacobsen SD, Hu MY, Chow P, Kung J, Liu H, Mao H-K, Hemley RJ (2005) Spin transition of iron in magnesiowüstite in the Earth's lower mantle. Nature 436:377-380

Mao H, Takahashi T, Basset WA, Weaver JS, Akimoto S (1969) Effect of pressure and temperature on the molar volumes of wüstite and the $(Mg,Fe)_2SiO_4$ spinel solid solution. J Geophys Res 74:1061-1069

Marquardt H, Speziale S, Reichmann HJ, Frost DJ, Schilling FR (2009) Single-crystal elasticity of $(Mg_{0.9}Fe_{0.1})O$ to 81 GPa. Earth Planet Sci Lett 287:345-352

Matsui M, Ito E, Yamazaki D, Yoshino T, Guo X, Shan S, Higo Y, Funakoshi K-I (2012) Static compression of $(Mg_{0.83},Fe_{0.17})O$ and $(Mg_{0.75},Fe_{0.25})$ O ferropericlase up to 58 Gpa

and 300, 700, and 1100 K. Am Mineral 97:176-183

Mayama N, Suzuki I, Saito T, Ohno I, Katsura T, Yoneda A (2005) Temperature dependence of the elastic moduli of ringwoodite. Phys Earth Planet Int 148:353-359

Mizutani H, Hamano Y, Ida Y, Akimoto S (1970) Compressional-wave velocities of fayalite, Fe_2SiO_4 spinel and coesite. J Geophys Res 75:2741-2747

Nakamura A, Schmalzried H (1983) On the nonstoichiometry and point defects of olivine. Phys Chem Minerals 10:27-37

Navrotsky A (1977) Calculation of the effect of cation disorder on silicate spinel phase boundaries. Earth Planet Sci Lett 33:437-442

Navrotsky A (1994) Physics and Chemistry of Earth Materials. Cambridge University Press

Nestola F, Ballaran TB, Koch-Müller M, Balic-Zunic T, Taran M, Olsen L, Princivalle F, Secco L, Lundegaard L (2010) New accurate compression data for γ-Fe_2SiO_4. Phys Earth Planet Int 183:421-425

Olinger B, Halleck PM (1976) The compression of α-quartz. J Geophys Res 81:5711-5714

Plymate TG, Stout JH (1990) Pressure-volume-temperature behavior of fayalite based on static compression measurements at 400º C. Phys Chem Minerals 17:212-219

Plymate TG and Stout JH (1994) Pressure-volume-temperature behavior of γ-Fe_2SiO_4 (spinel) based on static compression measurements at 400º C. Phys Chem Minerals 21:413-420

Rigden SM, Jackson I (1991) Elasticity of germinate and silicate spinels at high pressure. J Geophys Res 96:9999-10006

Schrettle F, Kant Ch, Lunkenheimer P, Mayr F, Deisenhofer J, Loidl A (2012) Wüstite: electric, thermodynamic and optical properties of FeO. Eur Phys J B 85:164 (12pp)

Sinogeikin SV, Bass JD, Kavner A, Jeanloz R (1997) Elasticity of natural majorite and ringwoodite from the Catherwood meteorite. Geophys Res Lett 24:3265-3268

Skinner BJ (1962) Thermal expansion of ten minerals. In Geological Survey Research 1962, Short Papersin Geology, Hydrology and Topography, article 152, D109-D112

Smyth JR (1975) High temperature crystal chemistry of fayalite. Am Mineral 60:1092-1097

Solomatova NV et al (2016) Equation of state and spin crossover of (Mg,Fe)O at high pressure, with implications for explaining topographic relief at the core-mantle boundary. Am Mineral 101:1084-1093

Speziale S, Duffy TS, Angel RJ (2004) Single-crystal elasticity of fayalite to 12 GPa. J Geophys Res B 100:12202

Sumino Y (1979) The elastic constants of Mn_2SiO_4, Fe_2SiO_4 and Co_2SiO_4 and the elastic properties at high temperature. J Phys Earth 27:209-238

Suzuki I, Ohtani E, Kumuzawa M (1979) Thermal expansion of γ-Mg_2SiO_4. J Phys Earth 27:53-61

Suzuki I, Seya K, Takei H, Sumino Y (1981) Thermal expansion of fayalite (Fe_2SiO_4). Phys Chem Minerals 7:60-63

Wang H, Bass JD, Rossman GR (1989) Elastic properties of Fe-bearing pyroxenes and olivines (abstract), EOS Trans. AGU 70:474

Wang J, Mao Z, Jiang F, Duffy TS (2015) Elasticity of single-crystal quartz to 10 GPa. Phys Chem Minerals 42:203-212

Wehringer B, Bosak A, Chumakov A, Mirone A, Winkler B, Dubrovinsky L, Dubrovinskaia N, Brazhkin V, Dyuzheva T, Krisch M (2013) Lattice dynamics of coesite. J Phys Condens Mat 25:275401 (8pp)

Weidner DJ, Carleton HR (1977) Elasticity of coesite. J Geophys Res 82:1334-1346

Welche PRL, Heine V, Dove MT (1998) Negative thermal expansion in beta-quartz. Phys Chem Minerals, 26, 63-77

Williams Q, Knittle E, Reichlin R, Martin S, Jeanloz R (1990) Structural and electronic properties of Fe_2SiO_4-fayalite at ultrahigh pressures: amorphization and gap closure. J

Geophys Res 95:21549-21563

Wood BJ, Kleppa OJ (1981) Thermochemistry of forsterite-fayalite olivine solution. Geochim Cosmochim Acta 45:529-534

Yagi T, Marumo F, Akimoto S (1974) Crystal structures of spinel polymorphs of Fe_2SiO_4 and Ni_2SiO_4. Am Mineral 59:486-491

Yagi T, Ida Y, Sato Y, Akimoto S (1975) Effect of hydrostatic pressure on the lattice parameters of Fe_2SiO_4 olivine up to 70 kbar. Phys Earth Planet Int 10:348-354

Zaug JM, Abramson EH, Brown JM, Slutsky LJ (1993) Sound velocities in olivine at Earth mantle pressures. Science 260:1487-1489

Zha C-s, Duffy TS, Downs RT, Mao H-k, Hemley RJ (1998) Brillouin scattering and X-ray diffraction of San Carlos olivine: direct pressure determination to 32 GPa. Earth Planet Sci Lett 159:25-33

Zhang L (1998) Single crystal hydrostatic compression of $(Mg,Mn,Fe,Co)_2SiO_4$ olivines. Phys Chem Minerals 25:308-312

Zhang J, Kostak Jr P (2002) Thermal equation of state of magnesiowüstite $(Mg_{0.6}Fe_{0.4})O$. Phys Earth Planet Int 129:301-311

Zhang JS, Hu Y, Shelton H, Kung J, Dera P (2016) Single X-ray diffraction study of Fe_2SiO_4 fayalite to 31 GPa. Phys Chem Minerals 44:171-179